ISSN 1063-780X, Plasma Physics Reports, 2016, Vol. 42, No. 4, pp. 369–381. © Pleiades Publishing, Ltd., 2016.
Original Russian Text © V.F. Tarasenko, E.Kh. Baksht, D.V. Beloplotov, A.G. Burachenko, M.I. Lomaev, 2016, published in Fizika Plazmy, 2016, Vol. 42, No. 4, pp. 376–390.

LOW-TEMPERATURE PLASMA

Amplitude–Temporal Characteristics of a Supershort Avalanche Electron Beam Generated during Subnanosecond Breakdown in Air and Nitrogen

V. F. Tarasenko[a, b], E. Kh. Baksht[a], D. V. Beloplotov[a, b], A. G. Burachenko[a, b], and M. I. Lomaev[a, b]

[a] *Institute of High Current Electronics, Siberian Branch, Russian Academy of Sciences, Tomsk, Akademicheskii pr. 2/3, Tomsk, 634055 Russia*

[b] *National Research Tomsk State University, pr. Lenina 36, Tomsk, 634050 Russia*

e-mail: vft@loi.hcei.tsc.ru

Received August 27, 2015; in final form, October 12, 2015

Abstract—The amplitude–temporal characteristics of a supershort avalanche electron beam (SAEB) with an amplitude of up to 100 A, as well as of the breakdown voltage and discharge current, are studied experimentally with a picosecond time resolution. The waveforms of discharge and SAEB currents are synchronized with those of the voltage pulses. It is shown that the amplitude–temporal characteristics of the SAEB depend on the gap length and the designs of the gas diode and cathode. The mechanism for the generation of runaway electron beams in atmospheric-pressure gases is analyzed on the basis of the obtained experimental data.

DOI: 10.1134/S1063780X16040085

1. INTRODUCTION

This year marks the 50th anniversary of work [1], in which generation of runaway electrons (REs) during a pulsed breakdown of atmospheric-pressure helium in a gap with a nonuniform electric field distribution was established for the first time by detection of X-ray bremsstrahlung. The results of that work experimentally proved Wilson's idea [2] about the possibility of electrons acceleration in gases under the action of a strong electric field when the energy gained by electrons between collisions with gas molecules and atoms exceeds collisional loses. In [2], the possibility of generating high-energy electrons in atmospheric-pressure discharges was predicted. X-ray emission during a pulsed discharge in atmospheric-pressure air was observed for the first time in [3]. Later, not only X-ray emission, but also an RE beam were observed in atmospheric-pressure air and other gases [4, 5].

RE generation in high-pressure gases is a fundamental physical phenomenon resulting, in particular, in the formation of a diffuse discharge without an external ionizing source providing gas preionization [4–10]. To date, there are several hundred publications on the generation of RE beams and X-ray emission in laboratory discharges at atmospheric pressure (see monograph [6], collection of papers [7], collective monograph [8], reviews [9, 10], and references therein). However, the results obtained in different research groups differ substantially. In addition, in new works, the earlier results are refined. For example, in [4] RE prints on an X-ray film were interpreted as X-ray ones. This led to an overestimation of the number of X-ray photons. Only in the subsequent work [5] of those authors, an RE beam in atmospheric-pressure air was detected using a Faraday cup. In [5], generation of RE beams was also observed in helium and other gases.

There are various reasons for the difference in the results of RE studies obtained by different authors. First, the duration of the RE beam is very short ($\sim 10^{-10}$ s) and depends on the experimental conditions, which makes it difficult to correctly measure the amplitude and duration of the RE beam current even using modern oscilloscopes. The duration and amplitude of the RE beam current pulse depend on the designs of the gas diode and cathode, the amplitude and rise time of the voltage pulse, and the kind and pressure of the gas. For example, the parameters of the RE beam under nonoptimal conditions can vary from pulse to pulse by more than an order of magnitude due to instability of the amplitude and rise time of the voltage pulse applied across the gas diode. In addition, the RE beam parameters measured behind the anode foil can also be unstable even for the same parameters of the voltage pulses because of changes in the state of the cathode surface that occur in atmospheric-pressure air and nitrogen in each pulse due to the formation of cathode spots. Second, detection systems with an insufficient time resolution were used in the experiments performed before 2005. Therefore, it was impossible to measure the electric characteristics of

the discharge with a subnanosecond time resolution and directly measure the parameters of the RE beam. To correctly measure the electric characteristics of the discharge, it is necessary to use voltage dividers, low-inductance shunts, collectors, connectors, cables, attenuators, and oscilloscopes with a sufficiently wide (>6 GHz) transmission band. Third, the results of measurements can substantially depend on the measurement methods. As a consequence, the results obtained in different research groups may differ considerably even when using similar devices. For example, in [5, 6, 11, 12], where a nonoptimal design of the gas diode and cathode were used, the numbers of electrons in the RE beam was found to be $(6–9) \times 10^8$, while in [13, 14], it was $(5–6.2) \times 10^{10}$. There is no consensus on the RE energy distribution. It was asserted in [6, p. 183] and [11] that the RE energy distribution reached its peak value at an energy of 290 keV for a gap length of 2 cm and gap voltage of $U_m = 190$ kV. Moreover, according to [6, 11] a monoenergetic RE beam with electron energies exceeding eU_m (where U_m is the amplitude of the gap voltage and e is the electron charge) is mainly generated in atmospheric-pressure air. Note also that, in [12], the results obtained by the same authors were changed. The peak in the RE energy distribution was downshifted to 270 keV [12, p. 269], while the gap voltage was increased to 270 keV [12, p. 264].

In our works [15–18], it was shown that, upon applying voltage pulses from the SLEP-150, SLEP-150M, and RADAN-220 pulsers across a gap filled with atmospheric-pressure air, the energy spectrum of REs downstream the anode foil consists of two to three groups of electrons with different energies. The main group of electrons have energies lower than eU_m (usually, by a few tens of keV), while the number of electrons with energies higher than eU_m does not exceed 10% of the total number of REs (for the case of a spherical cathode). In addition, there are a large number of electrons with energies from several units to several tens of keV. On the basis of RE absorption curves in foils, the authors of [19] asserted that the maximum RE energy does not exceed eU_m.

The aim of the present work was to perform detailed experimental studies of the amplitude–temporal characteristics of the discharge and RE beam generated during a subnanosecond breakdown in atmospheric-pressure gases with the highest possible time resolution and to determine the time at which REs appear behind the anode foil.

Here, we also compare the main results obtained by the research groups that contributed most to the experimental studies of the generation of RE beams in atmospheric-pressure air. This is rather important, because the earlier mistakes are often repeated in recent works; see, e.g., [11], where erroneous data on the RE spectrum were given. It was reported by the authors of [11] that they studied picosecond pulses, although their diagnostic equipment did not allow them to record pulses even with a duration of 100 ps. We propose to refer to RE pulses with a full width at half-maximum (FWHM) of 1–50 ps as picosecond ones, while to those with an FWHM of 50–500 ps as subnanosecond ones.

2. EXPERIMENTAL SETUP AND MEASUREMENT METHODS

The parameters of the RE beams generated during subnanosecond breakdowns in air, nitrogen, and other gases were studied using experimental setups consisting of the SLEP-150 [13, 17], SLEP-150M [9, 14, 17], and RADAN-220 pulsers [20]; discharge chambers; and a detection system.

Figure 1 shows the design of the output of the RADAN-220 pulser with a gas diode, shunt, and collector. The negative voltage pulses produced by the pulsers were applied via short transmission line *1* to electrode *4* with a small curvature radius. The voltage was measured using capacitive voltage divider *2*, located upstream the discharge gap. The RADAN-220 pulser formed voltage pulses with an amplitude of about 250 kV in the idle mode. The FWHM of the voltage pulse at a matched load is ≈2 ns, and the rise time of the voltage pulse in the transmission line is ≈0.5 ns. The discharge current was measured using current shunt *10*, made of thin-film low-inductance chip-resistors. Stainless-steel potential electrode (cathode) *4* had the shape of a cone with a vertex angle of 82° and base diameter of 6 mm. The radius of the curvature of the cone vertex was ~0.1 mm. In some experiments, a 6-mm-diameter tubular electrode made of a 100-μm-thick stainless-steel foil, as well as an electrode made of a sewing needle, was used. Flat grid (or foil) grounded electrode (anode) *6* was placed at a distance of 4–16 mm from the edge of potential electrode *4*. When using a grounded grid electrode, 10- or 50-μm-thick Al foil *7* was placed in front of the collector in order to suppress the displacement current. On this setup, the RE beam was detected using collector *8* with 20-mm-diameter receiving area *9*.

Figure 2 shows the design of the output of the SLEP-150 pulser, the gas diode, and the collector with a 3-mm-diameter receiving area. One electrode of the high-voltage line of pulser *1* is the case of peaking spark gap *2*. This allowed us to decrease the length of the line and form a voltage pulse of an amplitude of about 150 kV and FWHM of ≈1 ns at a matched load. The voltage pulse rise time was determined by the peaking spark gap and was ≈250 ps at a level of 0.1–0.9 at the optimal operation of the latter. Gas diode *5* was connected to high-voltage line *1* through short transmission line *3* with a wave impedance of 100 Ω. The amplitude of the voltage pulse in the transmission line depended on the breakdown voltage of peaking spark gap *2* and, with different peaking spark gaps, could vary from 120 to 200 kV. In the idle mode, the voltage

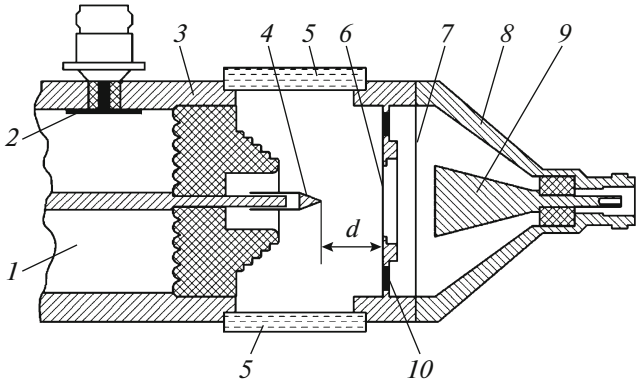

Fig. 1. Schematic of the output of the RADAN-220 pulser with the gas diode, shunt, and collector: (*1*) transmission line, (*2*) capacitive voltage divider, (*3*) insulator, (*4*) conical cathode, (*5*) quartz windows, (*6*) foil or grid anode, (*7*) Al foil, (*8*) collector case, (*9*) 20-mm-diameter receiving part of the collector, and (*10*) thin-film low-inductance chip resistors.

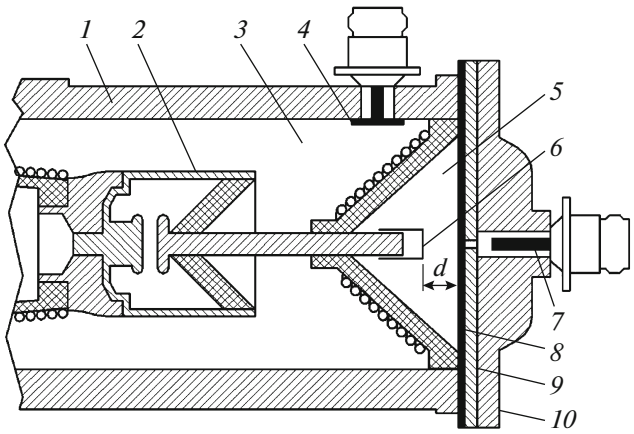

Fig. 2. Schematic of the output unit of the SLEP-150 pulser, gas diode, and collector with the 3-mm-diameter receiving area: (*1*) high-voltage line of the pulser, (*2*) peaking spark gap, (*3*) transmission line, (*4*) capacitive voltage divider, (*5*) gas diode, (*6*) tubular cathode, (*7*) receiving part of the collector, (*8*) foil, (*9*) 5-mm-thick collimator with a 1-mm-diameter hole, and (*10*) collector case. On the left, several turns of the high-voltage coil of the pulsed transformer are shown. On the right, the inductance coil connecting the inner electrode of the transmission line to the pulser case is shown on the insulator.

amplitude was doubled upon the arrival of the voltage pulse to the gas diode. In this device, different types of cathodes were used: 6-, 7-, and 20-mm-diameter tubular cathodes made of a 100-μm-thick stainless-steel foil, conical cathodes with a vertex angle of 82° and base diameter of 6 mm, needles, and a sphere with a diameter of 9.5 mm. A 3-mm-high ring with a 30- or 40-mm-diameter bottom on the edge of which 0.2-mm-diameter wires were stretched parallel to one another with a step of 4 mm was also used as a grid cathode. The distance from the wires to the bottom of the grid cathode was 1.5 mm. The design of such a cathode with a diameter of 40 mm was described in detail in [14]. The anode of the gas diode was made of 10-μm-thick aluminum foil *8*, which was reinforced with grid or collimator *9* from the side of the collector. In some experiments, the foil was replaced with a grid with a transparency of 14, 18, or 64% for light. The RE beam current (the number of electrons) was measured using collectors with 3- and 20-mm-diameter receiving areas. The total number of electrons in the RE beam behind the foil was measured using a 56-mm-diameter collector. The time resolutions of the collectors with the 3- and 20-mm-diameter receiving areas reached 20 and 80 ps, respectively. Capacitive voltage divider *4* was placed in the output of the pulser, which was filled with transformer oil. The distance from the capacitive divider to the end of the gas diode, to which the foil or grid was fixed, was 22 mm. The gap length d could be varied from 0 (shortcut circuit) to 24 mm.

Some experiments were performed with the SLEP-150M pulser, which had an additional transmission line with built-in capacitive voltage dividers. In this case, it was possible to measure both the incident (propagating from the pulser) voltage pulse and that reflected from the gas diode. This allowed us to recover the gap voltage with a higher accuracy than in measurements with capacitive divider *4* (Fig. 2). In some experiments with the SLEP-150M pulser, a transmission line with an air-filled cutting spark gap was used [21]. This made it possible to form voltage pulses with FWHMs of 0.1 and 0.2 ns. The gas diodes were usually filled with atmospheric-pressure air. We also performed experiments with other gases: nitrogen, helium, neon, argon, krypton, xenon, CH_4, and SF_6.

Signals from the capacitive voltage divider, current shunt, and the collector were recorded using LeCroy WaveMaster 830Zi-A (30 GHz, sampling time of 12.5 ps) and Tektronix DSA72504D (30 GHz, sampling time of 10 ps) digital oscilloscopes. The signals were transferred to the oscilloscope through 1-m-long RG58-A/U (Radiolab) high-frequency cables with Suhner 11 N-50-3-28/133 NE and SMA (Radiall R125.075.000) connectors. To attenuate the signals, 142-NM (Barth Electronics) high-frequency attenuators with a transmission band of up to 30 GHz were applied. When the RE beam current was measured by the collector with the 3-mm-diameter receiving area, the electric signal from it was transmitted to the oscilloscopes without attenuators. The oscilloscopes were triggered by the signal from the capacitive voltage divider. The voltage, discharge current, and RE beam current pulses were measured simultaneously during one pulse. The RE beam and X-ray emission were also detected using an RF-3 film enveloped in 120-μm-thick black paper. The discharge plasma glow was photographed using a Sony A100 digital camera.

It was proposed in [22] to call the RE beam detected behind the foil anode a supershort avalanche

electron beam (SAEB). Below we will use this term. The use of the term SAEB is substantiated in [23]. Note that the pulsers, collectors, and methods of measurements of the SAEB current and voltage pulses applied across the gas diode were described in detail in our previous works [8–10, 13–18, 21–27], as well as in [19, 28, 29], while no schemes of the magnetic spectrometer, the transition unit between the gas diode and magnetic spectrometer, the Faraday cup, the shunt, and other important components substantially affecting on the results of parameter measurements were given in [6, 11, 12] and other publications of that research group.

3. EXPERIMENTAL RESULTS AND DISCUSSION

3.1. Observed Forms of Discharge in Atmospheric-Pressure Air and Nitrogen

The form of the discharge excited after applying a nanosecond voltage pulse to a gap with a nonuniform distribution of the electric field depends on the gap length d [4–10]. At large values of d, a diffuse corona discharge forms near the cathode. As d decreases, the diffuse discharge fills the entire gap and the brightness of its glow increases. In [22], this discharge mode was proposed to be called an RE preionized (REP) diffuse discharge (DD). The REP DD was discussed in detail in [8]. Figures 3a and 3b show photographs of the glow of REP DDs in nitrogen and air obtained on the setup with the RADAN-220 pulser (see Fig. 1). An atmospheric-pressure diffuse discharge forms in both nitrogen and air. Bright spots appear only on the cathode with a small curvature radius. Short anode-directed spark leaders growing from the cathode spots are also seen. In the gas diode filled with nitrogen, the diffuse discharge is visually more uniform and contacts the side surface of the tubular cathode (Fig. 3a). It is seen in the photograph of the REP DD in air that the diffuse discharge consists of separate jets (Fig. 3b).

Figure 3c shows a photograph of the integral REP DD plasma glow taken from the side of the grid anode on the setup with the SLEP-150 pulser. A bright glow consisting of diffuse jets, which are closed on the grid, is observed near the tubular cathode. When the plasma glow of an REP DD in atmospheric-pressure nitrogen or air is observed through the side window (Figs. 3a, 3b), the glows of separate jets in the integral photographs overlap and become almost indistinguishable. As the gas pressure increases, the diameters of separate diffuse jets decrease and they become visible when being observed through the side window (see [8]). At pressures below the atmospheric one, the diffuse jets overlap and they are usually not seen in the integral photographs. The bright spots from which diffuse jets emerge are seen at the cathode edge (Fig. 3c), as in Figs. 3a and 3b. Short small-diameter diffuse jets that do not reach the grid are also observed. In Fig. 3c, a low-intensity air glow is also observed in the region of the gas diode remote from the cathode. It is seen from Fig. 3c that the axial region of the gap with a diameter nearly equal to that of the tubular cathode has the lowest glow intensity. However, at $d = 12$ mm, no decrease in the blackening of the RF-3 film near the axis of the gas diode with the 6-mm-diameter tubular cathode was observed in the print of the RE beam (Fig. 3d). The difference between the regions of the REP DD plasma glow and the print of the electron beam is due to the fact that the SAEB is generated starting with about 300 ps after applying the voltage pulse to the gap and has a duration of about 100 ps, whereas the plasma glow lasts for several tens of nanoseconds and reaches its maximum intensity about 500 ps after SAEB generation [8–10]. In addition, the SAEB electrons are emitted into a wide angle, due to which the size of the beam print increases substantially [9]. As the diameter of the tubular cathode increases, both the film blackening and the SAEB current density near the diode axis decrease [17].

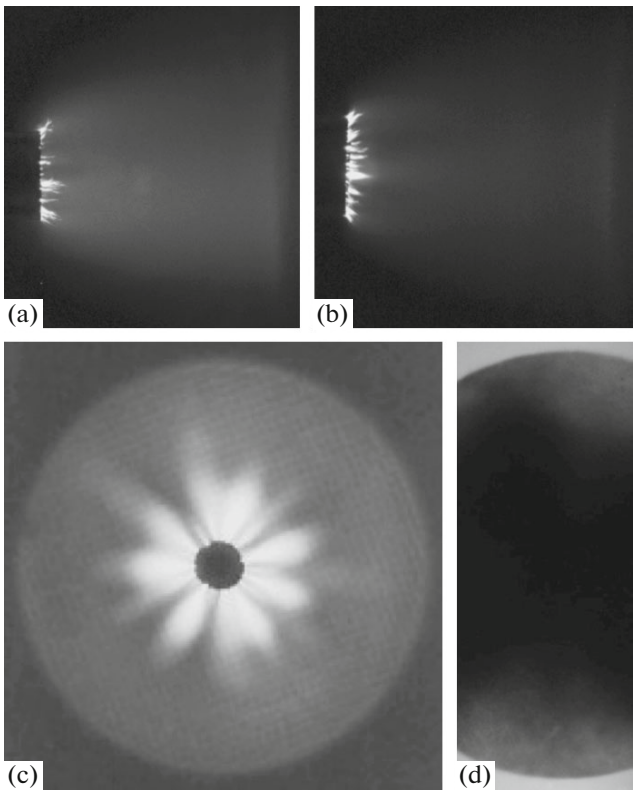

Fig. 3. Photographs of the discharge plasma glow in (a) nitrogen and (b, c) air and (d) SAEB print on an RF-3 film, obtained in one pulse on the setups with (a, b) the RADAN-220 pulser and (c, d) the SLEP-150 pulser at a gas pressure in the diode of 1 atm with gap lengths of (a, b) 14 mm and (c, d) 11 mm. The diameter of the tubular cathode located on the left in frames (a) and (b) is 6 mm, and that of the tubular cathode located in the centers of frames (c) and (d) is 7 mm.

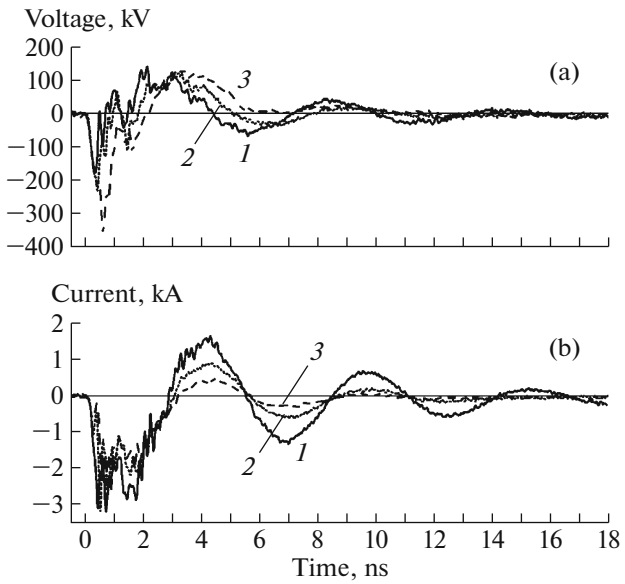

Fig. 4. Waveforms of the (a) voltage and (b) discharge current pulses. The cathode is a 6-mm-diameter tube. The gap length is d = (*1*) 6, (*2*) 12, and (*3*) 18 mm. The waveforms were obtained on the setup with the SLEP-150 pulser.

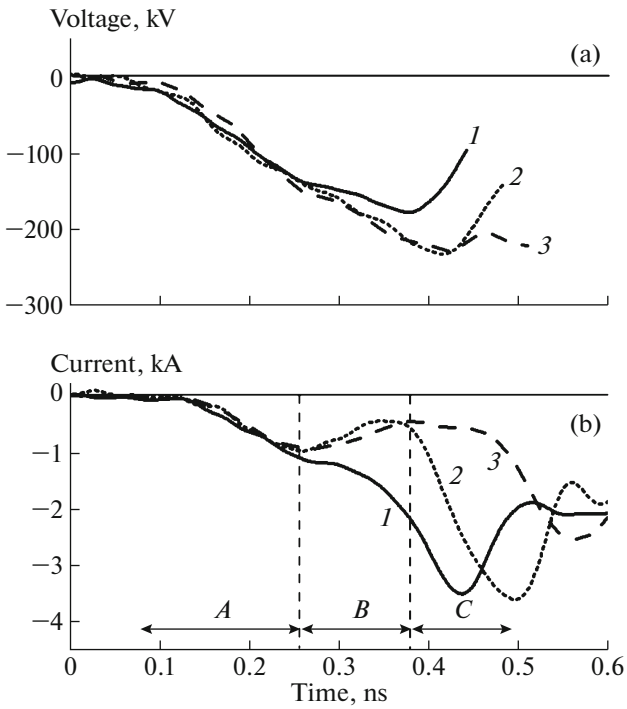

Fig. 5. Waveforms of the (a) voltage and (b) discharge current pulses obtained in the initial stage of the discharge on the setup with the SLEP-150 pulser. The cathode is a 6-mm-diameter tube. The gap length is d = (*1*) 6, (*2*) 12, and (*3*) 18 mm. Time intervals *A*, *B*, and *C* correspond to the current of the cold diode, dynamic displacement current, and conduction current, respectively.

At $d \leqslant 10$ mm, a cathode-directed spark leader formed against the background of the diffuse discharge on the setups with the SLEP-150, SLEP-150M, and RADAN-220 pulsers. As the gap length decreased, the spark leader transformed into a spark channel [30–33]. As d decreased further, the brightness of the spark channel increased and the diffuse discharge became almost invisible. However, our studies have shown that, at a nanosecond rise time of the high-voltage pulse, the discharge in a gap with a nonuniform electric field first operates in the diffuse mode and, then, constricts [8, 30–33]. As will be shown below, the SAEB is generated in the initial stage of the discharge, thereby providing REP DD formation.

3.2. Waveforms of the Voltage and Discharge Current Pulses

Figure 4 shows waveforms of the voltage pulses and the current through the gap for three values of d. When the REP DD forms on the setups with the RADAN-220 and SLEP-150 pulsers, the resistance of the diffuse discharge plasma is usually lower than the wave impedances of the pulsers. As a result, an oscillatory discharge mode takes place. At d = 12 and 18 mm, no more than five half-periods are observed in the waveform of the discharge current (Fig. 4b; curves *2*, *3*). As the gas pressure and/or the gap length d the increase, as well as when the gas diode is filled with electronegative gas SF_6, the resistance of the discharge plasma increases and an aperiodic discharge mode takes place.

At d = 6 mm (Fig. 4, curve *1*), the amplitude of the gap voltage, as was expected, decreased and both the amplitude of the discharge current and the number of current half-periods increased. The results obtained using an HSFC PRO high-speed four-channel CCD camera with the minimal exposure of 3 ns [31, 32] show that, at small values of d, the gap is bridged by the spark channel in several nanoseconds or less. This leads to an even larger decrease in the plasma resistance in the discharge gap and an increase in the number of oscillations of the discharge current. However, under these conditions, even at small d, the SAEB is observed in the beginning of the diffuse discharge stage before the formation of the spark channel.

Figure 5 demonstrates the initial segments of the voltage and current waveforms shown in Fig. 4. In these waveforms, obtained with a high time resolution, one can distinguish three typical discharge stages that were described for the first time in our works [9, 15, 34]. When the voltage pulse is applied to the gap, the well-known displacement current of a "cold" diode, equal to $C(dU/dt)$ (where C is the capacitance of the "cold" diode and U is the gap voltage), is first detected (time interval *A* in Fig. 5). By the "cold" diode we mean a diode in which there is still no dense plasma that "pushes out" the electric field. Note that Fig. 5 shows the voltage pulses measured by the capacitive

divider located at a distance of 22 mm from the anode of the SLEP-150 pulser. First, the divider detects the front of the incident wave. About 100 ps later, the front of the reflected wave reaches the divider, after which the divider measures the sum of these two waves. As a result, the waveform of the discharge current pulse in Fig. 5 is shifted with respect to the front of the voltage pulse by about 100 ps. At $d = 6$ mm, the displacement current continues to increase ≈250 ps after the voltage pulse has arrived at the capacitive divider, while dU/dt begins to decrease. The decrease in the dU/dt can be seen on the waveforms of the discharge current at $d >$ 10 mm. At $d = 12$ and 18 mm, the decrease in the displacement current is observed ≈250 ps after the arrival of the voltage pulse at the capacitive divider, while at $d = 6$ mm, the current through the gap continues to increase. Within time interval B (Fig. 5b), the current through the gap (curve *1*) slightly decreases and then increases. This is due to the contribution of the dynamic displacement current $U(dC^*/dt)$, caused by the charging of "compressing capacitor" C^*, formed by the edge of the dense plasma crossing the gap and the flat anode [35–37]. As was shown in [37], after the edge of the dense plasma reaches the anode, the second ionization wave with a higher velocity passes through the gap in the opposite direction. In this case, the current through the gap is determined by the conduction current (time interval C in Fig. 5b). At $d = 12$ and 18 mm, the discharge current (Fig. 5b; curves *2*, *3*) reaches its peak value later than at $d = 6$ mm (Fig. 5b, curve *1*). The time delays are about 50 and 100 ps, respectively. This is because, at larger values of d, a longer time is required for the ionization wave to traverse the gap.

Thus, the time evolution of the REP DD current includes three stages: the displacement current of the cold diode, the dynamic displacement current, and the conduction current. As will be shown below, the SAEB is generated mainly in the stage of the dynamic displacement current. It should also be kept in mind that, within time interval B, the current between the plasma edge and the anode is determined by the dynamic displacement current and the SAEB current, while that between the cathode and the edge of the dense plasma is determined by the conduction current. The current shunt records the sum of the dynamic displacement current and the SAEB current. These currents are difficult to separate, because the amplitude of the dynamic displacement current is, as a rule, much higher. For example, with the grid cathode, the amplitude of the dynamic displacement current reaches 2 kA [26].

3.3. Waveforms of the SAEB Current Pulses and Their Shift Relative to Those of the Voltage and Discharge Current Pulses

There are only two research groups in which the waveforms of the SAEB current behind the anode foil were measured with a time resolution of several tens of picoseconds (see [14, 24, 25] and [19, 28, 29]). However, only in our works [9, 15, 17, 34, 38], the waveforms of the SAEB current were synchronized with those of the voltage and discharge current pulses. For a time resolution of the detection system of ~100 ps, it is not difficult to synchronize the voltage in the idle mode with discharge current pulses. The displacement current of the cold diode and the front of the gap voltage are synchronous in time; hence, the peak of the displacement current corresponds to the maximum of dU/dt. To most exactly synchronize the waveforms of the voltage pulse at the gap and the discharge current, it is necessary to recover the gap voltage from the waveforms of the voltage pulses incident on the gap and reflected from it. To this end, the SLEP-150M pulser was equipped with an additional transmission line with built-in capacitive voltage dividers allowing one to measure the incident and reflected voltage pulses separately.

In these experiments, the waveforms of the SAEB current measured by the collector were synchronized with the waveforms of the discharge current and voltage pulse at the gap in the same way as in [9, 15, 17, 34, 38], i.e., by means of the displacement current of the cold diode. To this end, a grid anode was used, which made it possible to record the displacement current by the collector. Varying the size of the grid cell while keeping its transparency, it was possible to control the amplitude of the displacement current of the cold diode while keeping the amplitude of the SAEB current unchanged. In this way, it was possible to make the amplitude of the displacement current sufficient for synchronization with the front of the voltage pulse and, thereby, to synchronize the waveforms of the discharge current and SAEB current pulses with that of the voltage pulse. Note that the effect of the grid cell size on the value of the displacement current was not taken into account in [12], which, along with the low resolution of the detection system (in [12], a TDS 3052B oscilloscope with a bandwidth of 500 MHz was used), led the authors of [12] to the erroneous conclusion on the detection of an electromagnetic pickup in our works. The dynamic displacement current in [4–6, 11, 12] could not be measured because of the insufficient time resolution of the oscilloscope, the Faraday cup, and the shunt made of TVO resistors.

In the present work, as in [9, 15, 34, 37, 38], the amplitude of the dynamic displacement current was comparable with that of the SAEB current measured by the collector when a specially selected grid was used as an anode. To determine the time of SAEB generation, the signals from the collector behind the foil anode and the grid anode were recorded at the same voltage pulses and/or discharge current pulses. This allowed us to determine the position of the SAEB current pulse with respect to other pulses with an accuracy of several tens of picoseconds.

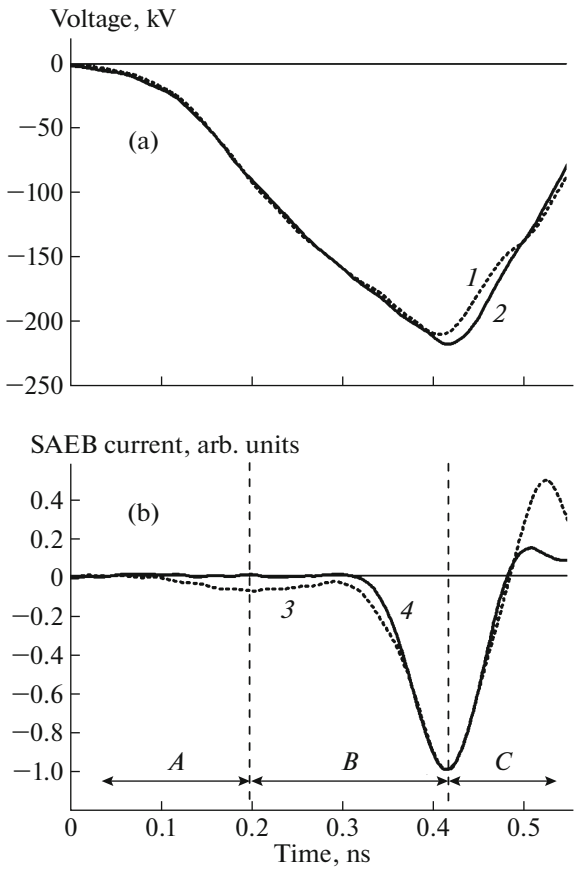

Fig. 6. Waveforms of the (a) voltage and (b) SAEB current pulses. The SAEB was detected by the collector with the 20-mm-diameter receiving area. Curves *1* and *3* were obtained on the setup with the SLEP-150 pulser by using a grid anode with a transparency of 64%, while curves *2* and *4*, by using an anode made of a 10-μm-thick aluminum foil. The cathode is a 6-mm-diameter tube. The gap length is $d = 12$ mm. Time intervals *A*, *B*, and *C* correspond to the current of the cold diode, dynamic displacement current, and conduction current, respectively.

Figure 6 presents an example of synchronization of the waveform of the SAEB current pulse with that of the voltage pulse when using the grid (Fig. 6; curves *1*, *3*) and foil (Fig. 6; curves *2*, *4*) anodes. In Fig. 6 (as in Fig. 5), signals from the capacitive voltage divider of the SLEP-150 pulser located at a distance of 10 mm from the cathode edge are shown. In this case, the front of the incident voltage wave was detected ≈60 ps earlier. Due to the special choice of the grid transparency and the grid cell size, the amplitudes and trailing edges of the collector signals obtained with the grid and foil anodes are determined by the SAEB current. A large-amplitude positive spike in the waveform of the collector signal (Fig. 5b, curve *3*) after the SAEB pulse in the case of the grid anode is associated with the effect of the positive charge of ions, which remain near the anode after REs escape through the grid. In the case of the grid anode, the initial segment of the collector signal (Fig. 6b, time interval *A*) is related to the displacement current of the cold diode. Then, the collector detects the dynamic displacement current and the SAEB current (Fig. 6b, time interval *B*). As in the case of detection of the discharge current by the shunt (Fig. 5b), the dynamic displacement current at a gap length of 6 mm begins to be observed about 250 ps after the arrival of the voltage pulse at the capacitive divider. This means that, by this time, the first electrons have already been emitted from the cathode and the plasma begins to form in the gap and propagate toward the anode. It is assumed that, at gap lengths of 12 and 16 mm, the first REs also appear with a time delay of about 250 ps after the arrival of the voltage pulse at the capacitive divider and 200 ps after the appearance of the displacement current of the cold diode. However, as the gap length *d* increases, the formation rate of the dense plasma near the cathode decreases due to a decrease in the electric field strength with distance from the cathode. As a result, within time interval *B*, the current signal from the collector and shunt decreases (see Figs. 5, 6).

At $d = 12$ mm and atmospheric-pressure air, the peak of the SAEB current nearly coincides with the maximum of the voltage pulse (Fig. 6). It should be taken into account that the receiving area of the collector is located at a distance of 5 mm from the anode. Electrons with energies of ≈150 keV travel this distance over 30 ps. Thus, electrons in the peak of the SAEB current come from the foil anode only 30 ps earlier. In [15, 34], the energy of electrons of the main SAEB group for $d = 12$ mm, a tubular cathode, and a voltage amplitude of ≈170 kV was found to be ≈150 keV. Under the conditions of Fig. 6, the voltage amplitude was ≈220 kV, i.e., it was lower than that in the idle mode (which under these conditions exceeded 350 kV), but higher than in [15, 34]. The increase in the voltage amplitude leads to an increase in the electron energy and, accordingly, a faster arrival of SAEB electrons at the collector.

Figure 7 shows waveforms of the voltage and SAEB current pulses for different gap lengths *d*. The collector with the 3-mm-diameter receiving area and a 5-mm-thick collimator with a 1-mm-diameter hole were used to detect the SAEB pulse. As was shown in [24, 25], this allowed us to correctly measure the SAEM current pulse, the FWHM of which was ⩾25 ps. As *d* was reduced, the maximum gap voltage decreased and the time delay of the SAEB current pulse measured by the collector behind the foil anode with respect to the front of the voltage pulse reached its minimal value. In these experiments, the accuracy of mutual synchronization of different SAEB current pulses, as well as of different voltage pulses, was better than 10 ps. Furthermore, the synchronization accuracy of the SAEB current pulses to the voltage pulses was no worse than several tens of picoseconds.

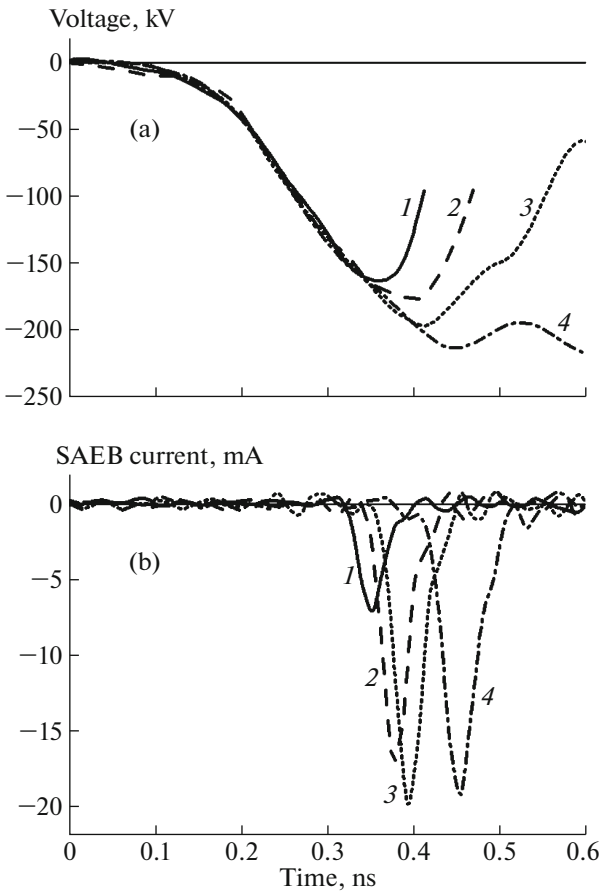

Fig. 7. Waveforms of the (a) voltage and (b) SAEB current pulses obtained on the setup with the SLEP-150 pulser. The SAEB was detected by the collector with the 3-mm-diameter receiving area, located behind a 5-mm-thick collimator with a 1-mm-diameter hole and a 10-μm-thick aluminum foil. The cathode is a 6-mm-diameter tube. The gap length is d = (*1*) 4, (*2*) 8, (*3*) 12, and (*4*) 16 mm.

An increase in the time delay of the SAEB current from the collector with increasing gap length can be associated with a slower formation of the dense plasma near the cathode and a slower passage of the front of the first ionization wave through the discharge gap. In addition, as the gap length increases, a longer time is required for the ionization wave to traverse the gap. In these experiments, the distance between the peaking spark gap and the anode plane was fixed and the gap length was varied by moving the tubular cathode in the gas diode along the cathode holder (the inner conductor of the transmission line, see Fig. 2). As a result, at a large gap length d, the incident voltage pulse arrived at the cathode edge earlier than at a small one. The voltage amplitude increases with increasing gap length. The increase in the breakdown voltage indicates that the formation rate of the dense plasma near the cathode and in the gap decreases with increasing gap length. In long gaps, the dynamic displacement current increases more slowly and a maximum is observed in the waveform of the displacement current of the cold diode (Figs. 5, 6). Under these conditions, the ionization wave bridges the discharge gap over a longer time. Accordingly, the voltage begins to decay later and the SAEB duration somewhat increases. In Fig. 7, the duration of the SAEB current pulse is the highest at d = 16 mm. It is seen from Fig. 7 that, for the 6-mm-diameter tubular cathode, a 12-mm-long gap is optimal for obtaining the largest SAEB amplitude. Measurements performed with the collector with a 20-mm-diameter receiving area also show that the SAEB currents is maximum at d = 12 mm. An increase in the length of the sharp cathode edge (as well as the use of a grid cathode and an increase in the diameter of the tubular cathode) leads to a decrease in both the optimal gap length and the gap voltage.

It is of interest to examine how the SAEB parameters depend on the propagation time of the voltage wave with a rise time of ~300 ps over the working surface of the grid cathode, with which the largest number of SAEB electrons was obtained [14]. Figure 8 shows waveforms of the SAEB current pulses passed through a 1-mm-diameter hole of the collimator that was located on the axis of the gas diode or displaced from the axis by 19 mm in the radial direction. A 30-mm-diameter grid cathode was used. Waveform *1*, obtained in one pulse, demonstrates the time resolution of the detection system. Among 50 waveforms, this is the waveform with the minimal (under these conditions) SAEB duration. Waveforms *2* and *3* are averaged over 25 pulses. Comparison of waveforms *1*, *2*, and *3* shows that the electron beams from the center of the cathode (waveform *3*) and from its peripheral area (waveform *2*) are generated simultaneously (to within 20 ps). The SAEB generation is more stable at the cathode periphery. In waveform *2*, the FWHM of the SAEB current pulse is smaller than in waveform *3* and is close to that in waveform *1*, obtained in one pulse.

3.4. Effect of the Collector, Collimator, and Cathode on the Amplitude and Duration of the SAEB Current

Direct detection of an SAEB pulse with an FWHM of ~100 ps, which corresponded to the actual SAEB duration, was reported for the first time in [39]. The SAEB duration was measured using a collector with a time resolution of ~50 ps and corresponded to the limiting time resolution of the TDS-6604 oscilloscope (6 GHz, sampling time of 50 ps) used in [39]. To resolve the leading and trailing edges of the SAEB current pulse, it is necessary to have at least three sampling points within them. For the sampling time of 50 ps, the minimal resolvable durations of the leading and trailing edges of the pulse are 100 ps. For a triangular SAEB pulse, this corresponds to the 100-ps-long FWHM. As was shown later in [14, 17], this duration was nearly equal to the durations of SAEB pulses

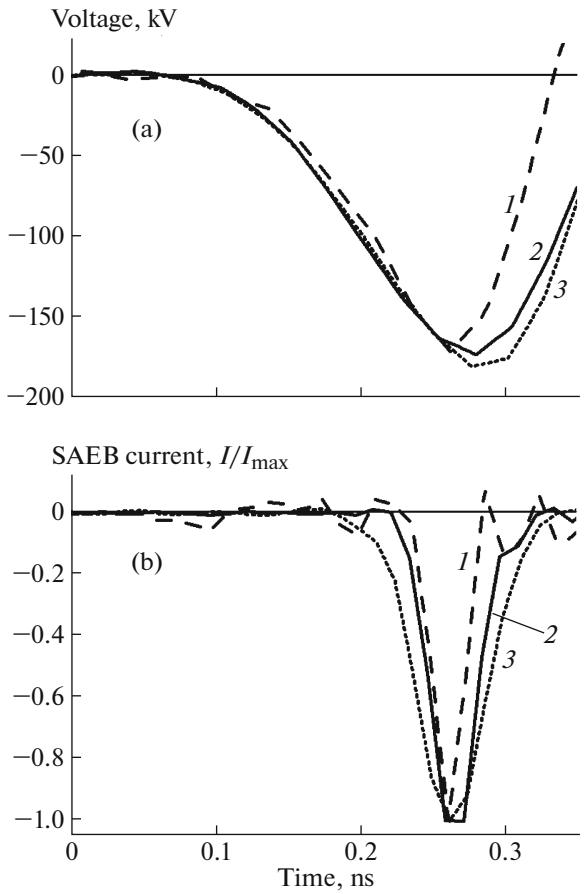

Fig. 8. Waveforms of the (a) voltage and (b) SAEB current pulses obtained on the setup with the SLEP-150 pulser. The SAEB was detected by the collector with the 3-mm-diameter receiving area, located behind a collimator with a 1-mm-diameter hole and a 10-μm-thick aluminum foil. Waveform *1* is obtained in one pulse, while waveforms *2* and *3* are averaged over 25 pulses. The collimator hole is located (*1*, *3*) on the axis of the gas diode and (*2*) at a distance of 19 mm from the axis. The gap length is $d = 6$ mm. The cathode is a grid fixed on a 30-mm-diameter ring.

detected behind the gas diode foil under similar conditions.

Figure 9 shows waveforms of SAEB current pulses obtained with different collectors and cathodes and different collimators. The SAEB current pulse shown in Fig. 9a was measured by the collector with the 3-mm-diameter receiving area behind a 5-mm-thick collimator with a 1-mm-diameter hole. For a spherical cathode and a gap length of 6 mm, the FWHM of the SAEB was ≈25 ps. The minimal durations of the SAEB current pulses were achieved with spherical and conic cathodes for gap lengths as short as 2–6 mm. The SAEB duration increases with increasing gap length and when using a tubular cathode with the length of the emitting edge of 19 mm. The FWHM of the SAEB current pulse shown in Fig. 9b is ≈40 ps. The duration of the SAEB pulse became even longer when the diameter of the collimator hole increased, while the collimator thickness decreased (Figs. 9c–9e). The FWHM of the SAEB pulse was ≈45 ps when using a 250-μm-thick copper collimator with a 4-mm-diameter hole (Fig. 9c).

The SAEB current pulse with the FWHM of ≈80 ps shown in Fig. 9d demonstrates the resolution capability of the collector with a 20-mm-diameter receiving area. The pulse from a considerable part of the anode foil detected by the collector behind a copper collimator with an 18-mm-diameter hole (Fig. 9e) has a typical SAEB pulse duration of ≈100 ps. SAEB pulses with similar durations were also observed when using cathodes of different design, as well as in discharges in atmospheric-pressure nitrogen and other gases. This unambiguously indicates that the duration of SAEB pulses behind the anode foil of a gas diode is ≈100 ps, rather than less than 50 ps, as was stated in [11, 40]. For the first time, a decrease in the SAEB duration with decreasing collector dimensions was observed in [41]. As the thickness of the anode foil increased, the duration of the SAEB pulse changed insignificantly when using collectors with both 3- and 20-mm-diameter receiving areas.

Note that, under certain conditions, a decrease in the parameter U/pd (where p is the gas pressure) [42–44] or the screening of the sharp cathode edge [28] led to the generation of an SAEB consisting of two pulses. The time interval between the maxima of these pulses exceeded 100 ps, due to which they could be measured using the collector with the 20-mm-diameter receiving area. The formation of two pulses can be explained by a relatively small (~20%) decay of the gap voltage during the generation of the first pulse and the passage of the second ionization wave from the cathode [42, 43] during the secondary voltage decay. It is assumed that the second pulse is generated due to electron emission from the front of the second ionization wave, which propagates from the cathode. Due to a decrease in the gap voltage, the electron energy in the second pulse is lower than in the first one and the FWHM of the second pulse is larger. When an SAEB consisting of two pulses is generated, its amplitude decreases.

As was noted in the Introduction, the parameters (amplitude and duration) of the SAEB current can vary from pulse to pulse. The strongest variations are observed under nonoptimal conditions and also when using a freshly manufactured cathode. Therefore, before experiments, the cathode was trained over several tens of pulses. Note that, here, for illustration, we present SAEB pulses obtained at identical voltage pulses and, when using a collimator with a 1-mm-diameter aperture, SAEB pulses of the same shape. In our previous works [24, 44–47], SAEB pulses having two to three peaks with a time interval between peaks of ≈30 ps were recorded with a picosecond time resolution. The reliability of detection of SAEB pulses with an FWHM of ≈25 ps, as well as the picosecond resolu-

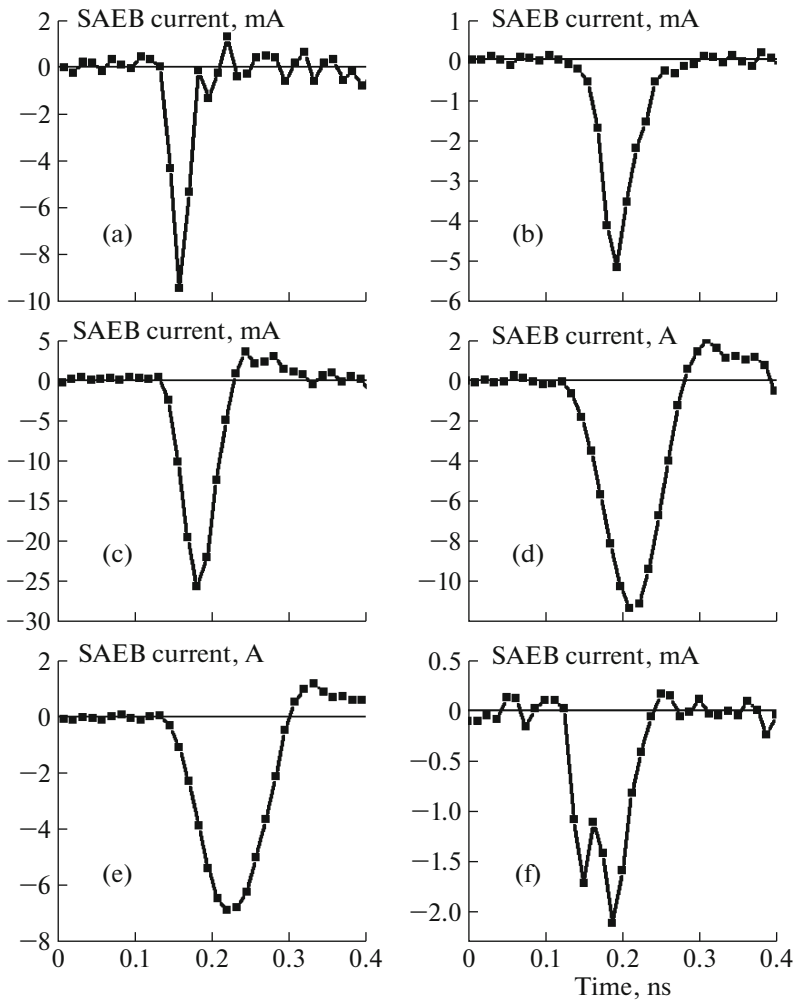

Fig. 9. Waveforms of the SAEB current pulses obtained using a collector with (a–c, f) 3- and (d, e) 20-mm-diameter receiving area, located behind a collimator with (a, b, f) 1-, (c) 4-, and (d, e) 18-mm-diameter hole. The cathode is (a) a sphere and (b–f) a tube. The gap length is d = (a) 6 and (b–f) 12 mm.

tion of the detection system consisting of the collector, cables, and connectors, is confirmed by measurements of the amplitude, phase, and frequency characteristics of the detection system by using an Agilent Technologies E8363B vector network analyzer in the frequency range of 0.01–40 GHz [47]. An example of a double-peak SAEB pulse is given in Fig. 9f. Such waveforms were most often observed with a tubular cathode at gap lengths shorter and longer than the optimal one. Double-peak pulses were also observed behind thick foils. We consider that two and more peaks are generated due to picosecond time delays between the formation of separate diffuse jets near the cathode and their subsequent propagation (see Fig. 3c). Since the gap voltage in this case changes insignificantly, double-peak pulses are observed behind thick foils. As the collimator hole increases, the RE fluxes from separate jets are mixed and the double-peak structure of the SAEB current becomes unobservable. Furthermore, due to mixing of electrons from separate jets and an insufficient time resolution, the double-peak structure is difficult to resolve by the collector with the 20-mm-diameter receiving area even with the use of a collimator.

The largest SAEB current amplitudes in atmospheric-pressure air were recently obtained with the SLEP-150 pulser at an amplitude of the incident voltage wave of 200 kV and a cathode made of wires stretched in parallel on a 40-mm-diameter ring [14]. The number of electrons in the beam reached 6.2×10^{10}, which corresponds to the SAEB current amplitude of 100 A at an FWHM of ~100 ps. In those experiments, a gas diode similar to that shown in Fig. 2 was used. Specific features of this diode are that it has the minimal inductance of the junction between the transmission line and the diode and that the entire side surface of the gas diode is covered with an insulator. When the side surface of the gas diode is partially open, the SAEB amplitude decreases. This is achieved

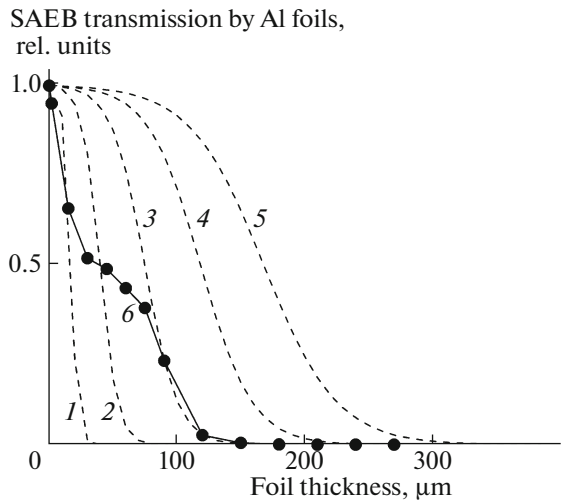

Fig. 10. Calculated numbers of electrons behind aluminum foils of different thickness for monoenergetic beams with different electron energies: (*1*) 50, (*2*) 100, (*3*) 150, (*4*) 200, and (*5*) 250 keV, and experimental SAEB attenuation curve obtained for $d = 12$ mm on the setup with the SLEP-150M pulser with a tubular cathode at $U_m = 170$ kV.

by decreasing the insulator length or applying a gas diode the side surface of which is not covered with an insulator (Fig. 1). The decrease in the SAEB current amplitude can be caused by the escape of a substantial fraction of REs onto the open part of the side surface of the gas diode. The application of an internal conical insulator (Fig. 2) results in the arrival of REs generated in the lateral direction [9, 34] at its inner wall and the charging of its surface. Apparently, this additional electric field of the negative surface charge of the insulator increases the number of REs arriving at the anode. The smallest SAEB amplitudes were observed with a needle cathode.

3.5. Energy of SAEB Electrons

The RE energy spectra were previously studied in our works [15–18]. Those studies, as well as results obtained with a high time resolution [25], unambiguously indicate the presence of two to three groups of electrons with different energies in an SAEB generated under conditions close to the optimal ones. The energy distribution of the main (the second according to our classification) group of electrons usually has a maximum at an energy that is lower by several tens of keV than eU_m. Note that, in most experiments with a subnanosecond rise time of the voltage pulse, electrons of the main group are mainly detected. The electrons of the first group have relatively low energies, as a rule, a few tens of keV and less. To detect the electrons of this group, one should use thin ($\leqslant 20$ μm) aluminum anode foils. In our experiments with the SLEP-150M pulser [9, 34] and the RADAN-220 pulser [39], a considerable increase in the SAEB current amplitude was observed with decreasing foil thickness. An example of such a dependence is presented in Fig. 10, which, along with the experimental absorption curve, shows the calculated attenuations of monoenergetic electron beams in aluminum foils of different thicknesses. The calculations were performed by the formula taken from [48]. The experimental curve has two characteristic bends at energies of 30 and 140 keV, which confirm the presence of three groups of electrons with different energies.

The electrons of the third group have energies higher than eU_m. However, these electrons are small in number. In experiments with a spherical cathode (which, among all cathodes under study, was optimal for the generation of electrons with energies higher than eU_m), the number of such electrons did not exceed 10% of the total number of SAEB electrons. This result is confirmed by experiments with the use of a time-of-flight spectrometer [15]. Note that, with the use of a spherical cathode, the breakdown gap voltage increased and varied substantially from pulse to pulse.

Experiments with different gap lengths and anode foils of different thickness have shown that, as the gap length (and, accordingly, the gap voltage) increases, the fraction of electrons with elevated energies in the main group increases. However, the number of these electrons is less than the number of electrons in the SAEB at the optimal gap length. For example, it follows from the dependence of the number of electrons in the beam on the gap length d that, for the SLEP-150 pulser with a 20-mm-diameter tubular cathode and a 15-μm-think Al foil anode, the optimal value of d is 6 mm. For a 20-μm-thick Cu foil anode under the same conditions, the largest number of REs was obtained at $d = 14$ mm. Due to an increase in electron energy losses in the anode, it is necessary to rise the gap voltage in order to increase the SAEB current amplitude behind the foil. This was achieved by increasing d without varying the amplitude of the pulser voltage. Similar results were also obtained with the RADAN-220 pulser with the 6-mm-diameter tubular cathode. For instance, as the anode Al foil thickness increased from 10 to 100 μm, the SAEB current amplitude decreased 24-fold at $d = 8$ mm, sixfold at $d = 12$ mm, and only 2.8-fold at $d = 16$ mm, i.e., the fraction of electrons with elevated energies increased with increasing gap length. It is seen from Fig. 7 that the breakdown voltage under these conditions increases.

4. ON THE MECHANISM OF RE GENERATION

Time-resolved studies of the amplitude–temporal characteristics of the RE beams generated during subnanosecond breakdowns in atmospheric-pressure gases, as well as of those of the voltage and discharge current pulses, allow one to better understand the mechanism of RE generation in atmospheric-pressure air.

The detection of the dynamic displacement current at the front of the voltage pulse indicates that electrons emission from the cathode begins with a time delay of $\leqslant$250 ps and a dense plasma the front of which propagates toward the anode is produced in the gap. The critical field for the appearance of field-emission electrons in vacuum is higher than 10^7 V/cm [49], while the critical field for electrons to pass into the runaway mode in atmospheric-pressure nitrogen, according to the nonlocal criterion [7], is about one order of magnitude lower. Therefore, the first REs appear near the cathode with a small curvature radius immediately after the first electrons have been emitted from the cathode. If the main group of REs detected by the collector are formed from the first electrons, then the time during which the first REs cross the discharge gap can be found from the time delay between the moments of the appearance of the dynamic displacement current and the exit of SAEB electrons from the foil. In these experiments, this time was 100–200 ps. This experimental result can be compared with the calculated time during which an electron with an initial energy of 1 keV and a final energy of 100–200 keV crosses the gap with a static electric field in the collisionless mode. According to calculations, an electron with a final energy of 100 keV crosses a 1-cm-long gap over 140 ps, while that with a final energy of 200 keV, over $\approx$100 ps. Agreement between the experimentally determined time of flight of electrons through the 1-cm-long gap in atmospheric-pressure nitrogen and the time required for the ionization wave to cross this gap (which, according to our measurements [37], is also 100–200 ps) confirms the mechanism of SAEB generation proposed in [22]. According to this mechanism, most REs are generated after the formation of dense plasma near the cathode, during the propagation of the ionization wave from the cathode to the anode. Generation of most REs during the propagation of the ionization wave was substantiated in [9, 17, 37]. This mechanism is also confirmed by the simultaneous detection of the dynamic displacement current and the SAEB current.

The obtained results allow us to assume that electrons with final energies of several tens of keV near the anode are generated mainly when the front of the dense plasma approaches the anode. If these electrons gained energy near the cathode, then electrons with final energies of 20 keV would pass through the gap without collisions over a time of about 300 ps and the waveforms of the beam current would exhibit an increase in the trailing edge of the SAEB pulse. However, in the waveforms of the SAEB current collected from a considerable area of the anode foil (see Figs. 9d, 9e), the leading and trailing edges of the current pulses have nearly the same duration. However, an extension of the trailing edge of the current pulse is observed during the detection of the SAEB electrons that have passed through a collimator with a 1-mm-diameter hole (see Figs. 7, 9b). Such an extension of the trailing edges of the SAEB current pulses in Figs. 7 and 9 can be explained by relatively slow electrons (with energies of several tens of keV), which pass into the runaway mode at a larger distance from the cathode, arriving at the collector with a certain time delay.

5. CONCLUSIONS

The results of time-resolved measurements of the amplitude–temporal characteristics of RE beams generated during subnanosecond breakdowns in atmospheric-pressure gases, as well as of those of the voltage and discharge current pulses, allow us to draw the following conclusions.

1. Detection (when using a grid anode with a specially selected transparency and cell size) of the displacement current of a cold diode (which means that there is no dense plasma in the gap) and the dynamic displacement current (the charging current of a "compressing capacitor" formed by the flat anode and the front of the dense plasma propagating through the gap), along with measurements of the SAEB current by using a collector, makes it possible to synchronize the SAEB current pulses with the waveforms of the voltage and discharge current pulses with an accuracy of several tens of picoseconds.

2. In atmospheric-pressure air and nitrogen at voltage pulse amplitudes of several hundred kV, the FWHM of the SAEB current pulse behind the entire surface of the anode foil is $\approx$100 ps. When recording the SAEB current behind a small-hole collimator, it is possible to separate out a fraction of the RE beam and reduce the FWHM of the SAEB current pulse to $\approx$20 ps. SAEB pulses are promising as a means for testing detection systems and collectors.

3. The energy spectrum of the RE beam generated during a subnanosecond breakdown consists of two to three groups of electrons with different energies. The number of electrons in the third group (electrons with the energies of higher than eU_m) does not exceed 10% of the total number of SAEB electrons.

4. The picosecond structure of SAEB pulses (the presence of two or more peaks spaced in time for several tens of picoseconds) observed behind small-hole collimators is caused by the nonuniformity of electron emission from different regions of the cathode during the formation of diffuse jets propagating through the discharge gap.

5. Double-peak SAEB pulses are generated when the gap breakdown occurs via the propagation of two ionization waves starting from the cathode.

ACKNOWLEDGMENTS

We are grateful to I.D. Kostyrya and D.V. Rybka for their help in performing these experiments. This work was supported by the Russian Science Foundation, project no. 14-29-00052.

REFERENCES

1. S. Frankel, V. Highland, T. Sloan, O. Van Dyck, and W. Wales, Nucl. Instrum. Methods **44**, 345 (1966).
2. C. T. R. Wilson, Proc. Cambridge Philos. Soc. **22**, 534 (1924).
3. Yu. L. Stankevich and V. G. Kalinin, Sov. Phys. Doklady **12**, 1042 (1967).
4. L. V. Tarasova and L. N. Khudyakova, Sov. Phys. Tech. Phys. **14**, 1148 (1969).
5. L. V. Tarasova, L. N. Khudyakova, T. V. Loiko, and V. A. Tsukerman, Sov. Phys. Tech. Phys. **19**, 351 (1974).
6. L. P. Babich, *High-Energy Phenomena in Electric Discharges in Dense Gases: Theory, Experiment, and Natural Phenomena (ISTC Science and Technology Series, Vol. 2)* (Futurepast, Arlington, VA, 2003).
7. *Proceedings of the General Physics Institute, Russian Academy of Sciences,* Ed. by S. I. Yakovlenko (Nauka, Moscow, 2007), Vol. 63 [in Russian].
8. *Runaway Electrons Preionized Diffuse Discharges,* Ed. by V. F. Tarasenko (Nova Science, New York, 2014).
9. V. F. Tarasenko, E. Kh. Baksht, A. G. Burachenko, I. D. Kostyrya, M. I. Lomaev, and D. V. Rybka, Plasma Dev. Operat. **16**, 267 (2008).
10. D. Levko, Ya. E. Krasik, and V. F. Tarasenko, Int. Rev. Phys. **6** (2), 165 (2012).
11. L. P. Babich and T. V. Loiko, JETP Lett. **101**, 735 (2015).
12. L. P. Babich and T. V. Loiko, Plasma Phys. Rep. **36**, 263 (2010).
13. I. D. Kostyrya, E. Kh. Baksht, and V. F. Tarasenko, Instrum. Exp. Tech. **53**, 545 (2010).
14. I. D. Kostyrya, D. V. Rybka, and V. F. Tarasenko, Instrum. Exp. Tech. **55**, 72 (2012).
15. V. F. Tarasenko, E. Kh. Baksht, A. G. Burachenko, I. D. Kostyrya, M. I. Lomaev, V. K. Petin, D. V. Rybka, and S. V. Shlyakhtun, Plasma Phys. Rep. **34**, 1028 (2008).
16. E. K. Baksht, A. G. Burachenko, V. Yu. Kozhevnikov, A. V. Kozyrev, I. D. Kostyrya, and V. F. Tarasenko, J. Phys. D **43**, 305201 (2010).
17. V. F. Tarasenko, Plasma Phys. Rep. **37**, 409 (2011).
18. A. V. Kozyrev, V. Yu. Kozhevnikov, M. S. Vorobyev, E. Kh. Baksht, A. G. Burachenko, N. N. Koval, and V. F. Tarasenko, Laser Part. Beams **33**, 183 (2015).
19. G. A. Mesyats, M. I. Yalandin, A. G. Reutova, K. A. Sharypov, V. G. Shpak, and S. A. Shunailov, Plasma Phys. Rep. **38**, 29 (2012).
20. F. Ya. Zagulov, A. S. Kotov, V. G. Shpak, Ya. Ya. Yurike, and M. I. Yalandin, Prib. Tekh. Eksp., No. 2, 146 (1989).
21. V. F. Tarasenko, A. G. Burachenko, E. Kh. Baksht, I. D. Kostyrya, M. I. Lomaev, and D. V. Rybka, Instrum. Exp. Tech. **52**, 366 (2009).
22. V. F. Tarasenko, V. M. Orlovskii, and S. A. Shunailov, Izv. Vyssh. Uchebn. Zaved., Fizika, No. 3, 94 (2003).
23. E. Kh. Baksht, A. G. Burachenko, M. V. Erofeev, and V. F. Tarasenko, Plasma Phys. Rep. **40**, 404 (2014).
24. D. V. Rybka, V. F. Tarasenko, A. G. Burachenko, and E. V. Balzovskii, Tech. Phys. Lett. **38**, 657 (2012).
25. V. F. Tarasenko, E. Kh. Baksht, A. G. Burachenko, I. D. Kostyrya, and D. V. Rybka, Plasma Phys. Rep. **39**, 592 (2013).
26. T. Shao, V. F. Tarasenko, Ch. Zhang, D. V. Beloplotov, A. G. Burachenko, D. V. Rybka, I. D. Kostyrya, M. I. Lomaev, E. K. Baksht, and P. Yan, Rev. Sci. Instrum. **84**, 053506 (2013).
27. D. V. Beloplotov, M. I. Lomaev, D. A. Sorokin, and V. F. Tarasenko, Opt. Atmos. Okeana **27**, 316 (2014).
28. G. A. Mesyats, A. G. Sadykova, S. A. Shunailov, V. G. Shpak, and M. I. Yalandin, IEEE Trans. Plasma Sci. **41**, 2863 (2013).
29. K. A. Sharypov, M. R. Ul'masculov, V. G. Shpak, S. A. Shunailov, M. I. Yalandin, G. A. Mesyats, and M. D. Kolomiets, Rev. Sci. Instrum. **85**, 125104 (2014).
30. M. I. Lomaev, D. V. Rybka, D. A. Sorokin, V. F. Tarasenko, and K. Yu. Krivonogova, Opt. Spectrosc. **107**, 33 (2009).
31. T. Shao, V. F. Tarasenko, Ch. Zhang, E. Kh. Baksht, P. Yan, and Yu. V. Shut'ko, Laser Part. Beams **30**, 369 (2012).
32. V. F. Tarasenko, E. Kh. Baksht, A. G. Burachenko, and M. V. Erofeev, High Voltage Eng. **39**, 2105 (2013).
33. D. V. Beloplotov, M. I. Lomaev, D. A. Sorokin, and V. F. Tarasenko, Dev. Appl. Oceanic Eng. **3**, 39 (2014).
34. V. F. Tarasenko, E. Kh. Baksht, A. G. Burachenko, I. D. Kostyrya, M. I. Lomaev, and D. V. Rybka, Laser Part. Beams **26**, 605 (2008).
35. V. F. Tarasenko, E. Kh. Baksht, A. G. Burachenko, I. D. Kostyrya, M. I. Lomaev, and D. V. Rybka, Tech. Phys. **55**, 210 (2010).
36. V. F. Tarasenko, E. Kh. Baksht, A. G. Burachenko, M. I. Lomaev, D. A. Sorokin, and Yu. V. Shut'ko, Tech. Phys. **55**, 904 (2010).
37. V. F. Tarasenko, D. V. Beloplotov, and M. I. Lomaev, Plasma Phys. Rep. **41**, 832 (2015).
38. A. G. Burachenko and V. F. Tarasenko, Tech. Phys. Lett. **36**, 1158 (2010).
39. V. F. Tarasenko, S. A. Shunailov, V. G. Shpak, and I. D. Kostyrya, Laser Part. Beams **23**, 545 (2005).
40. G. A. Mesyats, V. G. Shpak, S. A. Shunailov, and M. I. Yalandin, Tech. Phys. Lett. **34**, 169 (2008).
41. V. F. Tarasenko, S. I. Yakovlenko, V. M. Orlovskii, A. N. Tkachev, and C. A. Shunailov, JETP Lett. **77**, 611 (2003).
42. E. Kh. Baksht, V. F. Tarasenko, M. I. Lomaev, and D. V. Rybka, Tech. Phys. Lett. **33**, 373 (2007).
43. E. Kh. Baksht, A. G. Burachenko, M. I. Lomaev, D. V. Rybka, and V. F. Tarasenko, Tech. Phys. **53**, 93 (2008).
44. V. F. Tarasenko, M. V. Erofeev, M. I. Lomaev, D. A. Sorokin, and D. V. Rybka, Plasma Phys. Rep. **38**, 922 (2012).
45. V. F. Tarasenko, D. V. Rybka, A. G. Burachenko, M. I. Lomaev, and E. V. Balzovsky, Rev. Sci. Instrum. **83**, 086106 (2012).
46. D. Levko, Ya. E. Krasik, V. F. Tarasenko, D. V. Rybka, and A. G. Burachenko, J. Appl. Phys. **113**, 196101 (2013).
47. E. V. Balzovsky, D. V. Rybka, and V. F. Tarasenko, Instrum. Exp. Tech. **58**, 640 (2015).
48. T. Tabata and R. Ito, Nucl. Instrum. Methods **127**, 429 (1975).
49. G. N. Fursey, *Field Emission in Vacuum Microelectronics* (Plenum, New York, 2005).

Translated by L. Mosina